metals

MDPI

Article

Extraction of Cobalt and Manganese from Ferromanganese Crusts Using Industrial Metal Waste through Leaching

Kevin Pérez [1], Norman Toro [2,*], Pedro Robles [3], Felipe M. Galleguillos Madrid [4], Edelmira Gálvez [5], Francisco Javier González [6], Egidio Marino [6], Jonathan Castillo [7], Ingrid Jamett [8] and Pía C. Hernández [1,8,*]

1 Departamento de Ingeniería Química y Procesos de Minerales, Facultad de Ingeniería, Universidad de Antofagasta, Antofagasta 1240000, Chile; kevin.perez@sqm.com
2 Faculty of Engineering and Architecture, Universidad Arturo Prat, Iquique 1110939, Chile
3 Escuela de Ingeniería Química, Pontificia Universidad Católica de Valparaíso, Valparaíso 2340000, Chile; pedro.robles@pucv.cl
4 Centro de Desarrollo Energético Antofagasta, Universidad de Antofagasta, Antofagasta 1240000, Chile; felipe.galleguillos.madrid@uantof.cl
5 Departamento de Ingeniería Metalúrgica y Minas, Universidad Católica del Norte, Antofagasta 1270709, Chile; egalvez@ucn.cl
6 Instituto Geológico y Minero de España (IGME-CSIC), Ríos Rosas, 23, 28003 Madrid, Spain; fj.gonzalez@igme.es (F.J.G.); e.marino@igme.es (E.M.)
7 Departamento de Ingeniería en Metalurgia, Universidad de Atacama, Copiapó 1531772, Chile; jonathan.castillo@uda.cl
8 Centro de Economía Circular en Procesos Industriales (CECPI), Facultad de Ingeniería, Universidad de Antofagasta, Antofagasta 1270300, Chile; ingrid.jamett@uantof.cl
* Correspondence: notoro@unap.cl (N.T.); pia.hernandez@uantof.cl (P.C.H.)

Abstract: Ferromanganese crusts are mineral resources distributed in the planet's oceans. These deep-sea minerals stand out for their abundance and diversity of metals, with Mn and Co being the most abundant elements. These minerals are a good alternative to diversify the extraction of elements, which today are found at low grades on the Earth's surface. For the co-processing of ferromanganese crusts to recover Co and Mn, there are few studies. These generally worked with the use of a reducing agent, and in many cases previous roasting processes. In the present investigation, two ferromanganese crusts that were collected from two seamounts in the central eastern Atlantic Ocean were characterized. Subsequently, these crusts were leached in an acid-reducing medium, adding steel waste (slag) with 99.73% Fe_3O_4 and 0.27% metallic iron from the steel industry as a reducing agent. Acid-reducing processes have previously been shown to yield high and rapid recoveries of Co and Mn from seabed minerals. However, there is no previous study using smelting slag as a reducing agent for the treatment of ferromanganese crusts. The best results of this research were obtained when working at 60 C, achieving joint extractions of Co and Mn of ~80% and ~40%, respectively, in 10 min. In addition, the process residues were analyzed, and the formation of contaminating elements or the precipitation of Co and Mn species was not observed.

Keywords: leaching; deep-sea mining; waste utilization; acid leaching; Co and Mn extraction; slags

Citation: Pérez, K.; Toro, N.; Robles, P.; Galleguillos Madrid, F.M.; Gálvez, E.; González, F.J.; Marino, E.; Castillo, J.; Jamett, I.; Hernández, P.C. Extraction of Cobalt and Manganese from Ferromanganese Crusts Using Industrial Metal Waste through Leaching. *Metals* **2024**, *14*, 1044. https://doi.org/10.3390/met14091044

Academic Editor: Daniel Assumpcao Bertuol

Received: 2 August 2024
Revised: 2 September 2024
Accepted: 6 September 2024
Published: 13 September 2024

1. Introduction

Ferromanganese (Fe-Mn) crusts represent a globally distributed mineral resource found in vast areas of the world's oceans [1,2]. These crusts appear at depths ranging from 400 to 7000 m, primarily covering the flanks of underwater seamounts, ridges, and plateaus [3,4]. Fe-Mn Crusts were formed during intervals devoid of volcanic activity and are characterized by minimal sedimentation at the seamount interface with substantial volumes of ocean water [5–7], originating through either hydrothermal-hydrogenic or hydrogenic-diagenetic processes, as illustrated in Figure 1 [8–10]. Fe-Mn crusts exhibit a porous surface, characterized by a dark brown or black hue, with a distinctive spherical

shape. Internally, these crusts display laminated, massive, columnar, and/or botryoidal textures. Ranging in thickness from 0.1 cm to 26 cm, the most substantial deposits rich in metals are typically encountered at depths ranging from 800 to 2500 m [11–13].

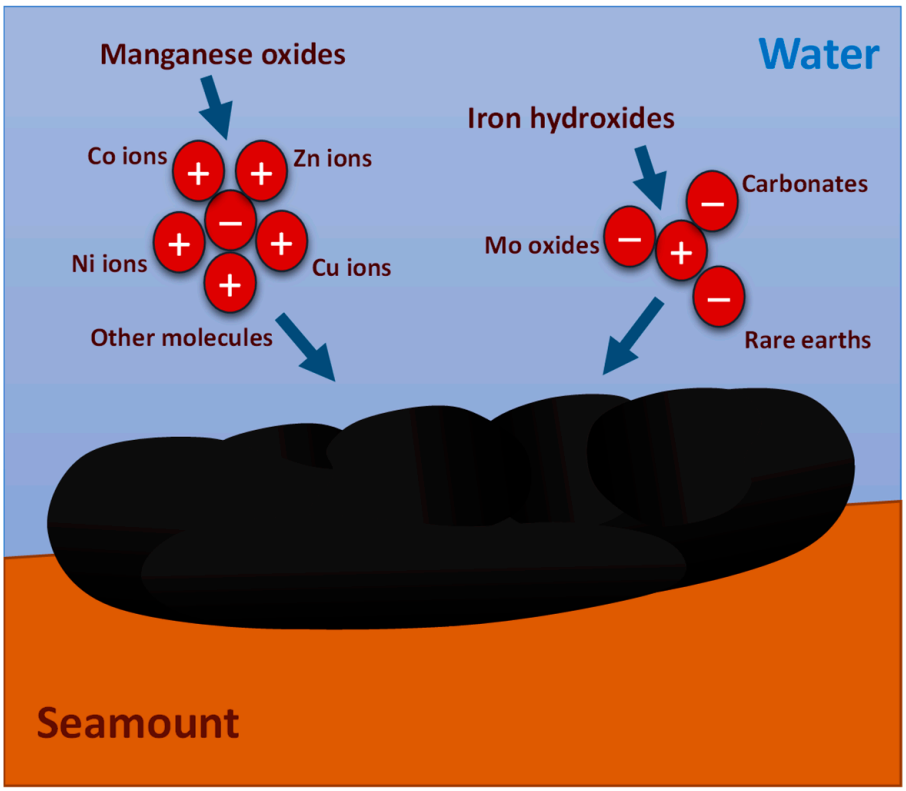

Figure 1. Formation of ferromanganese crusts (modified from [14]).

Undoubtedly, the principal attribute elevating the value of Fe-Mn crusts as a mineral resource lies in their remarkable abundance and diversity of metals, i.e., their polymetallic nature [15,16]. These include, but are not limited to, Co, V, P, Cd, As, Mo, Sr, Te, Ni, Ba [17–19] heavy and light rare earth elements, as well as the complete spectrum of platinum group elements [20–22], as outlined in Table 1.

The extensive array of elements present in Fe-Mn crusts plays a pivotal role in fostering the sustainable development of clean technologies, crucial for transitioning towards a reduction in carbon dioxide emissions. These technologies heavily rely on what are termed "critical raw materials", a group of 34 substances recognized for their significance and scarcity in terms of Earth's surface reserves. Notably, Fe-Mn crusts encompass over 10 of these 34 critical raw materials, as detailed in Table 2. The term "energy-critical elements" was created by a joint committee of the American Physical Society and Materials Research Society assembled in 2009 to investigate the material resources available to support emerging energy technologies [23,24]. Security of mineral supply has been identified by the European Commission as a priority challenge facing the raw materials sector.

Table 1. Representative chemical compositions of ferromanganese crusts within Canary Island Seamount Province exploration areas (adapted from [22]).

	Echo Seamount				Paps Seamount				Drago Seamount				Tropic Seamount								Atlantic Mean	Pacific Mean	Indian Mean
Sample	**DR2-9**	**DR3-1**	**DR04-14**	**DR7-8**	**DR9-10**	**DR9-11**	**DR10-7**	**DR11-2**	**DR14-1**	**DR13-11**	**DR13-12**	**DR13-13**	**DR15-14A**	**DR15-15**	**DR16-5**	**DR16-13**	**Mean**	**Min.**	**Max.**	**St. Dev.**	**n = 25 + 18 + 13**	**n = 2339**	**n = 14**
Fe (wt. %)	26.48	22.72	25.99	13.55	20.27	21.49	24.72	15.58	26.58	18.91	26.06	27.58	26.51	26.99	6.98	28.33	23.45	13.55	28.33	4.56	18.84	19.27	23.6
Mn	17.53	14.18	17.66	13.04	13.82	14.48	17.69	7.72	19.01	12.05	18.22	18.84	16.94	18.77	4.92	21.74	16.11	7.72	21.74	3.53	14.68	21.37	15.6
Mn/Fe	0.66	0.62	0.68	0.96	0.68	0.67	0.72	0.50	0.72	0.64	0.70	0.68	0.64	0.70	0.70	0.77	0.69	0.50	0.96	0.10	0.78	1.11	0.66
SiO_2	5.45	12.47	6.39	18.48	19.32	16.33	11.68	5.70	5.11	12.18	6.80	6.57	8.14	7.50	8.00	3.65	9.72	3.65	19.32	5.07	10.42	12.81	7.78
Al_2O_3	2.60	5.13	3.23	6.60	6.21	4.94	3.97	2.65	2.75	4.51	3.11	3.11	3.04	2.99	2.52	1.29	3.74	1.29	6.60	1.46	3.87	2.91	1.34
CaO	3.37	4.00	3.11	8.19	2.65	2.98	3.22	25.25	4.45	12.20	5.04	2.99	5.59	3.58	33.03	3.49	6.01	2.65	25.25	5.89	2.53	4.28	0.75
TiO_2	1.65	2.47	1.30	1.04	1.68	1.55	1.75	1.76	1.84	1.53	1.63	1.64	1.45	1.59	0.55	1.24	1.61	1.04	2.47	0.32	1.29	1.63	1015
K_2O	0.43	0.90	0.50	0.75	0.88	0.69	0.50	0.27	0.41	0.95	0.45	0.51	0.45	0.40	0.49	0.33	0.56	0.27	0.95	0.22	2.1	0.74	2.32
MgO	2.21	2.96	2.26	4.48	2.73	2.51	2.04	1.79	2.25	2.00	1.96	1.98	1.89	2.04	1.79	1.90	2.33	1.79	4.48	0.68	2.17	2.04	1.72
P_2O_5	1.32	1.71	1.25	3.78	1.17	1.28	1.20	0.84	2.01	6.40	1.15	1.12	1.19	1.21	18.08	1.09	1.78	0.84	6.40	1.46	1.43	1.56	0.38
Na_2O	1.70	1.62	1.56	1.67	1.93	2.47	1.76	1.13	1.81	1.50	1.52	1.94	1.58	2.12	1.38	1.77	1.74	1.13	2.47	0.31	1.9	2.32	2.24
H_2O	12.95	10.71	11.77	7.56	10.53	11.2	12.42	6.06	11.39	8.71	10.32	11.71	11.65	13.17	3.95	12.59	10.85	6.06	13.17	2.01	11.2	15.38	12.8
LOI	26.92	23.90	26.31	22.87	23.63	24.67	25.73	31.08	25.74	21.96	26.25	25.90	26.80	26.74	17.38	27.15	25.71	21.96	31.08	2.17	-	28.73	-
Co (μg/g)	5157	5375	4245	3560	4239	3767	4502	4230	6745	3359	4887	5090	3834	4664	1698	7169	4722	3359	7169	1086	3919.5	4770.75	3126
V	3072	2148	3143	1326	1862	2005	2465	1035	2446	1527	2568	2830	2643	2796	432	3614	2365	1035	3614	716	813.37	584	624
Zn	754	721	670	672	656	718	709	373	708	489	669	735	625	694	356	899	673	373	899	118	570.67	655.58	533
Ni	2443	2737	2252	6036	3238	2734	2756	1502	3558	1972	2420	2513	1994	2405	2481	2924	2766	1502	6036	1038	2326.85	3777.33	2558
Cu	476	539	261	1573	969	637	771	479	798	555	651	926	395	542	490	387	664	261	1573	321	798.78	892.42	1254
Mo	456	354	511	214	282	355	379	103	440	283	454	504	437	457	136	644	392	103	644	133	383.89	435.92	330
W	100	91	129	38	44	28	90	29	115	50	114	138	95	106	32	84	83	29	138	36.62	79.63	79.44	78
Pb	2284	1707	2224	826	1307	1486	1736	828	1762	1157	1658	1861	1595	1819	337	2106	1624	826	2284	445	1128.13	1502	1058
As	478	433	479	255	379	389	416	325	470	310	439	458	469	412	99	563	418	255	563	78	316.28	329.08	181
Tl	72	87	137	95	95	61	71	50	116	56	81	112	60	60	31	127	85	50	137	28	106.31	100.36	89.4
Ba	4525	2893	4673	1701	2474	2649	3510	1031	2061	3906	4601	2964	3480	4086	1015	5841	3360	1031	5841	1286	1407	1997	1668
Nb	98	138	97	116	119	100	125	154	122	100	101	123	89	88	27	85	110	85	154	20	52.67	36.17	74
La	380	343	397	172	222	276	330	189	422	330	390	412	374	402	364	402.3	336	172	422	83	265.26	292.25	286
Ce	1913	1663	1859	692	1329	1402	1694	1190	1773	1283	1834	2000	1762	1942	449.77	2176	1634	692	2176	386	1446.34	1157.08	1481
Pr	82.71	73.36	88.18	34.40	46.27	58.45	70.34	35.87	89.27	69.45	86.31	93.22	82.97	91.21	61	89.92	72.79	34.40	91.21	20	64.32	60.77	68.8
Nd	335	299	360	150	190	240	287	143	363	285	350	375	341	373	260.28	362	297	143	375	81	245.62	251.67	248
Sm	67.78	60.25	73.33	31.37	40.01	50.23	59.15	28.74	73.69	56.96	71.59	76.45	71.08	76.01	49.77	74.82	60.76	28.74	76.45	16.31	56.45	51.95	60.2
Eu	16.31	14.56	17.68	7.90	9.84	12.27	14.50	6.93	17.49	14.02	17.06	18.12	17.20	18.20	12.70	17.50	14.64	6.93	18.20	3.77	11.96	15.79	10.8
Gd	78.35	70.44	82.06	39.70	48.40	59.91	68.97	35.77	81.48	66.16	79.50	81.21	80.81	84.76	63.72	77.57	69.01	35.77	84.76	16.07	62.15	52.92	62
Tb	10.82	9.80	11.56	5.53	6.94	8.67	9.64	5.01	11.40	9.45	11.26	11.44	11.43	12.09	8.75	10.69	9.72	5.53	12.09	2.25	9.54	8.83	9
Dy	62.26	56.33	66.30	34.40	41.58	50.90	56.63	29.27	65.23	55.43	63.45	63.43	66.33	68.87	56	59.72	56.01	29.27	68.87	12.08	49.53	52.96	49.4
Y	199	220	239	225	171	209	201	120	264	285	226	219	246	229	557	173	215	120	285	40.10	167.31	179.75	163
Ho	11.95	11.12	12.81	7.33	8.30	10.34	11.06	5.82	12.75	11.06	12.04	11.89	12.79	12.90	12.49	11.07	10.88	5.82	12.90	2.13	9.7	9.53	9.8
Er	32.51	30.80	35.82	21.74	24.03	29.05	30.49	16.39	35.21	31.33	32.78	32.51	35.09	35.01	37.69	29.63	30.16	16.39	35.82	5.51	28.5	28.4	26
Tm	4.58	4.28	4.95	3.04	3.49	4.23	4.34	2.36	4.92	4.34	4.57	4.49	4.90	4.87	5.18	4.06	4.23	2.36	4.95	0.74	3.78	4.03	3
Yb	28.37	26.65	30.83	18.93	22.24	26.91	27.63	15.33	30.47	27.71	28.55	27.98	30.45	30.17	33.63	25.05	26.49	15.33	30.83	4.46	24.08	26.24	22.7
Lu	4.06	3.93	4.43	2.94	3.38	4.00	4.11	2.30	4.59	4.10	4.13	4.02	4.37	4.23	5.28	3.48	3.87	2.30	4.59	0.61	3.8	3.54	3.46
%REY	0.32	0.29	0.33	0.14	0.22	0.24	0.29	0.18	0.32	0.25	0.32	0.34	0.31	0.34	0.20	0.35	0.28	0.18	0.35	0.06	0.24	0.22	0.25
%HREY	13.9	15.5	15.40	25.3	15.7	17.0	14.9	13.1	20.1	14.9	13.8	16.2	16.2	14.8	40.1	11.7	15.5	11.7	25.3	3.22	15.13	17.40	14.35
Ce_{SN}/Ce_{SN}	2.48	2.41	2.28	2.06	3.01	2.53	2.55	3.30	2.10	1.95	2.30	2.35	2.30	2.33	0.68	2.63	2.44	1.95	3.30	0.35	2.41	1.89	2.3
Ce *	0.37	0.36	0.34	0.28	0.45	0.38	0.38	0.49	0.30	0.26	0.34	0.35	0.34	0.35	−0.21	0.40	0.36	0.26	0.49	0.06	0.4	0.26	0.38
Y_{SN}/Ho_{SN}	0.48	0.56	0.53	0.88	0.59	0.58	0.52	0.59	0.59	0.74	0.54	0.53	0.55	0.51	1.27	0.45	0.57	0.45	0.88	0.11	0.51	0.56	0.49

Table 1. *Cont.*

	Echo Seamount				Paps Seamount				Drago Seamount				Tropic Seamount								Atlantic Mean	Pacific Mean	Indian Mean
Sample	**DR2-9**	**DR3-1**	**DR04-14**	**DR7-8**	**DR9-10**	**DR9-11**	**DR10-7**	**DR11-2**	**DR14-1**	**DR13-11**	**DR13-12**	**DR13-13**	**DR15-14A**	**DR15-15**	**DR16-5**	**DR16-13**	**Mean**	**Min.**	**Max.**	**St. Dev.**	**n = 25 + 18 + 13**	**n = 2339**	**n = 14**
Ru ** (ng/g)	10.09	11.42	9.07	14.93	16.09	10.44	12.90	10.86	14.22	16.43	14.83	12.69	18.68	9.72	-	11.55	12.93	9.07	18.68	2.84	17.3	10.5	13
Rh **	10.55	15.90	8.81	16.12	17.55	9.16	12.79	18.20	17.49	19.72	21.41	13.82	12.79	9.89	-	14.76	14.60	8.81	21.41	3.92	30.8	13	24
Pd **	5.30	1.41	6.45	1.17	1.36	12.73	1.44	21.29	<DL	<DL	1.49	2.87	171	2.21	-	6.25	15.66	<DL	171	46.31	9.9	3.67	7
Os **	1.00	1.21	0.65	0.93	1.36	0.77	1.07	1.25	1.57	1.87	1.04	0.59	1.34	0.97	-	0.98	1.11	0.59	1.87	0.34	-	-	-
Ir **	3.19	3.80	2.74	3.99	4.27	2.65	3.59	4.27	4.33	4.94	5.45	3.78	3.66	3.09	-	3.96	3.85	2.65	5.45	0.76	5.8	4.08	8
Pt **	291	160	108	222	213	112	146	159	159	173	321	208	222	103	-	138	182	103	321	64	425	270.17	348

* calculated with methodology explained in Marino et al. [22]. ** Ce anomaly calculated as Ce * = Log (Ce/(2/3La + 1/3Nd)).

Table 2. Raw materials considered critical by the European Union in 2023.

Critical Raw Materials				
Antimony	Cobalt	Germanium	Natural Graphite	Light rare earths
Beryllium	Coke	Indium	Niobium	Heavy rare earths
Borates	Fluorspar	Magnesite	Platinum group	Silicon metals
Chromium	Gallium	Bismuth	Phosphate rocks	Tungsten
Lithium	Titanium	Strontium	Bauxite	Hafnium
Natural Rubber	Vanadium	Wolfram	Tantalum	Scandium
Copper	Manganese	Nickel		

It is essential to emphasize that overexploitation and the constant decrease in the grades of mineral deposits on Earth's surface have caused an increase in production by mining companies in order to counteract this situation [25–27]. However, this practice entails the creation of significant environmental liabilities, such as the accumulation of large quantities of land and underwater waste during flotation processes, which is the most widely used metal recovery method globally [28]. Moreover, the uneven distribution of critical metals across Earth's surface creates geopolitical tensions among major world powers. This is fueled by the limited supply available on the market in comparison to the soaring demand for these essential resources [6]. In response to the aforementioned scenario, underwater mining emerges as a promising alternative for metal extraction, with ferromanganese crusts standing out as a valuable resource for recovering cobalt and manganese. It is estimated that substantial quantities of these two elements are predominantly located in seabed reserves, making underwater mining an attractive prospect [29]. Limited research exists on the co-processing of ferromanganese crusts to extract cobalt and manganese. Typically, this involves leaching processes utilizing a reducing agent, with some instances incorporating preliminary roasting procedures.

Ju et al. [30] processed Fe-Mn crusts using a roasting method, incorporating sawdust as a reducing agent at a temperature of 723.15 K, followed by leaching at room temperature with a liquid/solid ratio of 10. The addition of sulfuric acid at a concentration of 0.5 mol/L resulted in impressive extractions, achieving 98.47% for cobalt and 99.32% for manganese within a 30 min timeframe. In another way, Inoue and Kawahara et al. [31] used an ammonia solution and SO_2 as a reducing agent at moderate temperature (60 °C), pulp density of 2 g/L, SO_2 150 mL/min, and ammonium carbonate at 1 mol/L, and extractions of 97% cobalt and 6% manganese were obtained in 120 min. Nakazawa and Sato [32] conducted bacterial leaching employing Thiobacillus ferrooxidans in an acidic medium (H_2SO_4), with elemental sulfur serving as the reducing agent and a pulp density of 0.1% (0.15 g of sample per 150 mL of leaching solution). Remarkably, researchers successfully extracted 90% cobalt and 70% manganese within an 18-day timeframe. Shibata et al. [33] worked with an acid-reducing medium, using H_2O_2 at 0.0365 mol/L, HCl at 0.1 mol/L, and 25 °C, achieving extractions of 90% Mn and 92% Co in 40 min. Furthermore, the researchers indicates that without the presence of an oxidizing agent, it was necessary to work at 3 mol/L of HCl and 30 °C to extract 95% Mn and 94% Co in 90 min. Niinae et al. [34] used ammonium sulfate and ammonium thiosulfate as reducing agents, ammoniacal solution $(NH_4)_2SO_3$ at a concentration of 0.1 mol/L, and temperature of 70 °C, achieving extractions of 63% Mn and 39% Co in 120 min.

Conversely, in the context of employing steel slag as a reducing agent in an acidic medium for the simultaneous dissolution of cobalt and manganese, a recent investigation conducted by Pérez et al. [29] offers valuable insights. Exploring the dissolution of marine nodules at ambient temperature reveals the feasibility of this process, as evidenced by the reactions outlined in Table 3. These reactions, characterized by highly favorable Gibbs free energy values, were employed in a recent study. The researchers achieved extractions of 80% manganese and 35% cobalt within a 15 min timeframe employing a reducing agent ratio of 1/2 (nodules/steel slag) at room temperature. Intriguingly, under identical conditions, but at an elevated temperature of 60 °C, extractions surged to 98% for manganese and 55% for cobalt within the same 15 min duration.

Table 3. Proposed reactions for the dissolution of cobalt and manganese from seabed minerals (adapted from [29]).

Reaction	ΔG° (kJ)	Equation
Fe_3O_4 (s) + $4H_2SO_4$ (l) = $FeSO_4$ (aq) + $Fe_2(SO_4)_3$ (s) + $4H_2O$ (l)	−264.27	(1)
$2FeSO_4$ (aq) + $2H_2SO_4$ (aq) + MnO_2 (s) = $Fe_2(SO_4)_3$ (s) + $2H_2O$ (l) + $MnSO_4$ (aq)	−221.44	(2)
$CoO + H_2SO_4 = CoSO_4 + H_2O$	−115.43	(3)
$Co_3O_4 + 4H_2SO_4 + 2FeSO_4 = 3CoSO_4 + 4H_2O + Fe_2(SO_4)_3$	−354.18	(4)

Chile has an exclusive economic zone (EEZ) of 4,264,560 km^2 with various underwater mineral resources, such as manganese nodules, underwater polymetallic sulfides, ferromanganese crusts, marine phosphorites, and submarine gas hydrates. In particular, for ferromanganese crusts, significant quantities are found in the volcanic ridge of which the Salas and Gómez, San Félix, and San Ambrosio islands are a part, and also the sedimentary basins that surround Easter Island, where these resources have significant concentrations of manganese (10%) [35]. On the other hand, Chile is a sulfuric acid-producing country and has extensive facilities for the treatment of minerals by hydrometallurgical means, which could be left unused due to the country's production plan for the year 2030 to increase the treatment of materials through flotation processes to compensate for the drop in copper grades by increasing production. For the reasons previously stated, it is necessary to look for new alternative sources of valuable elements for processing by hydrometallurgical routes that are less polluting to the environment compared to flotation and pyrometallurgy.

In the present manuscript, a novel acid-reductive leaching mechanism is proposed by reusing steel residue (slag) from the steel industry in Chile for the joint recovery of cobalt and manganese from ferromanganese crusts.

2. Materials and Methods

2.1. Ferromanganese Crusts

Samples Drago 0511/DR04-15 and Subvent 1/DA06-4 were recovered by dredge on the seamounts Echo and Gaire (central eastern Atlantic Ocean) during two cruises performed by the Geological Survey of Spain (IGME): Drago 0511 and Subvent 1 aboard the Spanish R/V *Miguel Oliver* and R/V *Hesperides*, respectively (Table 4).

Table 4. Sample location in the seamount, water depth and Fe-Mn crust thickness.

Sample	Seamount	Sample Location	Latitude	Longitude	Water Depth (m)	Fe-Mn Crust Thickness (mm)
Drago 0511/DR04-15	Echo	West flank	25°19.51′ N	19°18.92′ W	1832–1593	25
Subvent 1/DA06-4	Gaire	East flank	26°06.20′ N	22°09.00′ W	4823	64

The Echo and Gaire seamounts form part of the Canary Island Seamount Province, one of the biggest and most ancient volcanic and metallogenic provinces in the Atlantic Ocean [22]. Co-rich ferromanganese crust deposits cover the substrate rocks and sediments on the tops and flanks of the seamounts. Echo Seamount is a shallow guyot type seamount located in the southwest of the Canary Islands archipelago. Its morphology is represented by a flat top, summit at 253 m depth, and steeped slopes of different degrees. Guyot-type seamounts have this morphology due that during their history could be passed an islands period with sub-aerial and marine processes of erosion. Gaire Seamount is an elongated NNO-SSE volcanic submarine hill, along with a secondary smaller cone separated by a short east-west dorsal. This seamount rises from ca. 4900 m depth to 4600 m depth with stepped flanks and measuring 6 km in length and 5 km in width in the area of the secondary cone.

Mineralogical and petrographic analyses were conducted at IGME-CSIC laboratories on polished thin sections (ca. 30–120 μm thick) using a DM2700P Leica microscope (Leica, Wetzlar, Germany) coupled with a DFC550 digital camera. X-ray powder diffraction (XRD) was performed using a PANalytical X'Pert PRO diffractometer (Philips Analytical, Almelo, The Netherlands), with CuKα radiation, carbon monochromator and automatic slit. The analytical conditions were: CuKα radiation at 40 kV and 30 mA, a curved graphite secondary monochromator, scans from 2° to 70° (2θ), step size of 0.0170° (2θ) and step time 0.5°/min.

Bulk geochemistry of Fe and Mn was determined at IGME-CSIC using X-ray fluorescence (XRF) on PANalytical's Zetium (Malvern Panalytical, Almelo, The Netherlands) equipment with a rhodium tube and fused pearl preparation (SuperQ, Malvern Panalytical, Almelo, The Netherlands). The accuracy of the data was verified using international standard NOD-A-1 (USGS), and precision was found to be better than ±5%. Analytical conditions were 50 kV voltage and 50 mA. The obtained contents were compared with certified international standards.

Trace Co, Ni, Cu and REY (rare earth elements plus yttrium) were analyzed using inductively coupled plasma mass spectrometry (ICP-MS) (Agilent 7500 ce, Agilent Technologies, Santa Clara, CA, USA) and inductively coupled plasma atomic emission spectroscopy (ICP-AES) (Varian Vista-MPX, Varian Inc., Palo Alto, CA, USA) measurements for Co and Ni. For these techniques, samples were prepared with an ultrapure 3-acid digestion (HF, HNO_3, and HCl), dried until almost complete dryness, and the residuals were diluted with HCl 10%.

2.2. Iron Residue

The steel residue utilized, "slag" was sourced from the steel smelting operations of the CAP Company in Antofagasta, Chile. This residual material contained 82.65% Fe_3O_4, 13.03% Fe_2O_3, and 0.27% metallic iron (See Table 5). Initially ranging in size from 1 to 10 mm, it underwent size reduction in a mortar, resulting in particles sized between −140 and +100 μm.

Table 5. Chemical analysis of steel residue.

Element	Mass (wt. %)
Fe_3O_4	82.65
Fe_2O_3	13.03
Fe^0	0.27
CaO	0.75
SiO_2	1.5
Al_2O_3	0.3
MgO	0.2
SO_3	0.08
P_2O_5	0.2
K_2O	0.015
MnO	0.8
C	0.2

2.3. Leaching Test

The leaching tests were carried out in a 200 mL glass reactor at 0.1 solid-to-liquid ratio (100 mL of acid solution (H_2SO_4) and Fe-Mn crust/Fe(res) ratio of 1/2. A total of 10 g of the mineral (ferromanganese crust) was kept under agitation and suspension using a 5-position magnetic stirrer (IKA ROS, CEP 13087-534, Campinas, Brazil) at 600 rpm and a particle size of −177 to +149 μm. The temperature was controlled using an oil-heated circulator (Julabo, St. Louis, MO, USA). The temperature range tested in the experiments was 25 to 60 °C. All tests were performed in duplicate, and analyses were carried out using 5 mL undiluted samples and AAS with a ≤5% variation quotient and 5–10% relative difference. The pH and oxidation-reduction potential were measurements of the leaching solutions and were

carried out in a pH-ORP meter (HANNA HI-4222, St. Louis, MO, USA). The ORP solution was measured using an ORP electrode cell composed of a platinum-employed electrode and a saturated Ag/AgCl reference electrode.

3. Results and Discussion

3.1. Sample Characterization

The thickness of cobalt-rich ferromanganese crusts is 2.5 cm for Drago 0511/DR04-15 and 6.4 cm for Subvent 1/DA06-4. They show subspherical botryoids and sometimes current-smoothed upper surface with the appearance of typical hydrogenic crusts formed at the seafloor. Both crusts show a general internal layered pattern of typical black hue with a dark-brown layer covering volcanic rock substrate in the sample Subvent 1/DA06-4 and semi-consolidated carbonate sediments in the Drago 0511/DR04-15 (Figure 2). Polished sections of cut samples of crusts under the reflected light microscope show different internal structures: massive, dense to porous, and mottled.

Figure 2. Image of Fe-Mn crust samples selected for this study. (**A**) Crust Drago 0511/DR04-15 was dredged from Echo Sm. (**B**) crust Subvent 1/DA06-4 from Gaire Sm.

The crusts are composed of poorly crystalline Fe and Mn oxyhydroxides. Fe–vernadite is the main Mn mineral with minor amounts of other Mn oxides such as asbolane and goethite as the main Fe minerals (Figure 3). Light-colored and porous thin laminations intercalated between massive and dense textures, abundant in the sample Subvent 1/DA06-4, correspond essentially to siliciclastic detrital accumulation. In addition to Fe-Mn oxyhydroxides, microscopic and XRD studies show the presence of small amounts of minority minerals, represented essentially by silicates (detrital quartz and feldspars and authigenic clays), carbonates (authigenic calcite and bioclastic accumulation), and authigenic phosphates (carbonate fluorapatite).

Bulk chemistry of both crusts reflects the main mineralogy (Table 6), showing high average contents of Fe (19.6 wt. %) and Mn (15.1 wt. %) and lower amounts of the other major elements (in total <15%). The sample Subvent 1/DA06-4 shows major abundance of siliciclastic elements (SiO_2 13.8 wt. % and Al_2O_3 5.3 wt. %), and the sample Drago 0511/DR04-15 exhibits higher contents of elements linked to phosphates (CaO 6.05 wt. % and P_2O_5 2.47 wt. %) (Table 6). Among the trace elements, the crusts are enriched in many critical and strategic elements highlighted in this study: Co (up to 4262 µg/g), Ni (up to 2844 µg/g), Cu (up to 1342 µg/g), and rare earth elements plus yttrium (up to 2323 µg/g).

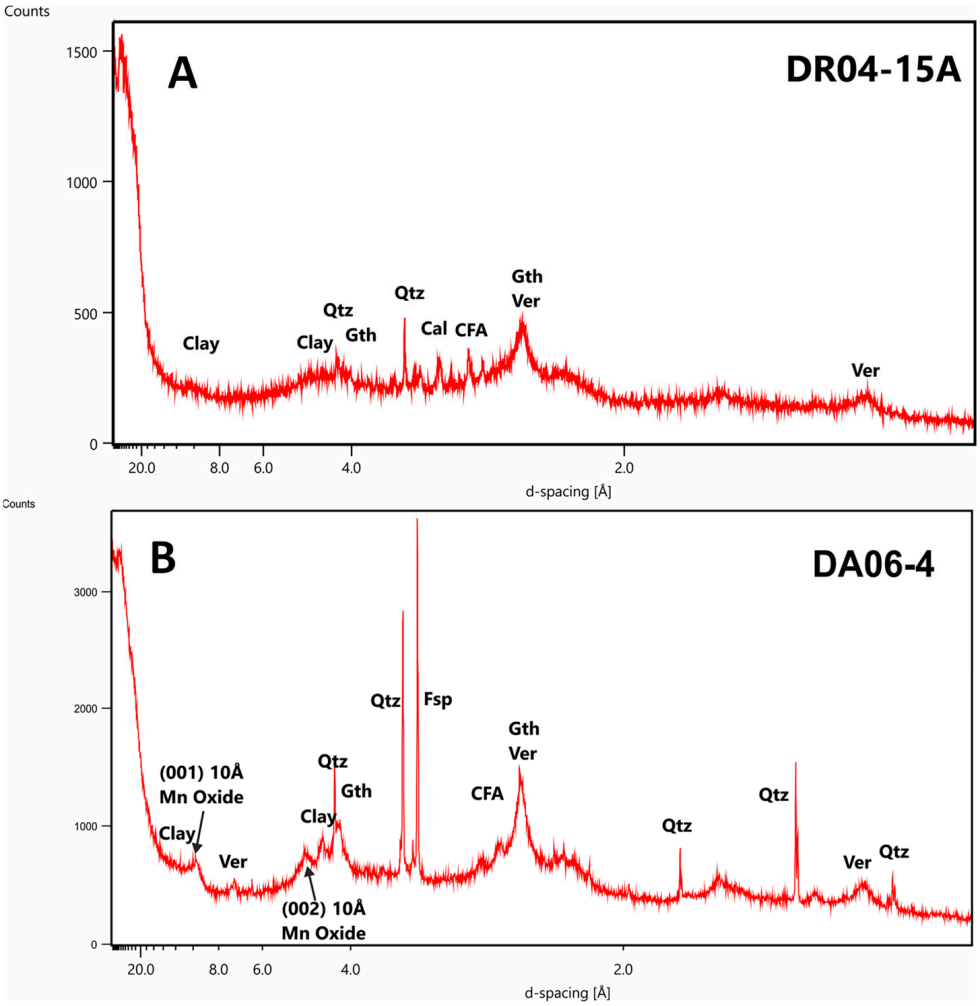

Figure 3. (**A**,**B**) X-ray diffraction (XRD) analysis of bulk samples. In samples Drago 0511/DR04-15 and Subvent 1/DA06-4, is possible recognize Fe oxyhydroxides represented by goethite-group (Gth) minerals and Mn oxides, essentially Fe-vernadite (Ver). In sample Subvent 1/DA06-4, it is also possible to recognize ~10 Å reflection due to the presence of todorokite (Tod), asbolane (Asb) or buserite (Bus), feldspars (Fsp) and peaks of carbonate-fluorapatite (CFA). Calcite (Cal) was detected in Drago 0511/DR04-15, and quartz (Qtz) peaks are shown in both samples.

Table 6. Bulk chemistry of samples in selected elements for this study.

Element	Drago 0511/ DR04-15A	SUBVEMT/ DA06-4	Element	Drago 0511/ DR04-15A	Subvent/ DA06-4
SiO_2 (wt. %)	6.91	13.80	Ag	0.17	<0.2
Al_2O_3	2.86	5.38	Cd	1.49	3.45
Fe_2O_3	28.43	27.70	Sb	46.02	31.75
Fe	19.88	19.37	Te	37.26	18.06
CaO	6.05	1.89	Ba	1374	1188
TiO_2	1.03	0.96	Tl	69.25	114.37
MnO	18.69	20.23	Pb	1566	859
Mn	14.47	16.66	Th	31.98	108.05
K_2O	0.47	0.83	U	11.49	8.71

Table 6. *Cont.*

Element	Drago 0511/ DR04-15A	SUBVEMT/ DA06-4	Element	Drago 0511/ DR04-15A	Subvent/ DA06-4
MgO	2.36	2.48	Y	169	134
P_2O_5	2.47	0.80	La	240	209
Na_2O	1.59	1.35	Ce	1420	1476
LOI	22.81	23.20	Pr	49.70	56.89
SUM	93.67	98.62	Nd	205.00	224.76
Mn/Fe	0.73	0.81	Sm	41.80	51.05
Be (μg/g)	8.87	6.48	Eu	10.20	12.19
V	940.67	674.22	Gd	49.50	53.57
Cr	25.03	19.78	Tb	7.04	7.74
Co	4262	2424	Dy	42.70	43.23
Ni	2359	2844	Ho	8.71	7.90
Cu	474	1342	Er	25.20	21.77
Zn	456	430	Tm	3.52	3.07
As	341	231	Yb	22.00	20.00
Se	21.06	29.56	Lu	3.41	3.00
Mo	383.89	376.52	ΣREY	2298	2323

The sum of the major elements and their LOI (loss on ignition) reach 94 and 98 wt. %, respectively, which is within the error calculated for this kind of sample, characterized by high hygroscopy. Humidity calculated before the LOI of both samples is 21.3% and 6.4% respectively.

3.2. Leaching Ferromanganese Crusts

Figure 4 and Table 7 illustrates the outcomes of the manganese and cobalt extraction from the studied ferromanganese crusts. The data reveal a positive correlation between the temperature of the system and the recovery of both elements, aligning with findings from prior studies on the dissolution of these elements from underwater resources [14,36]. Although there are no previous studies on recovering metals from ferromanganese crusts under the same operational conditions used in this research, a recent study undertook a project focused on extracting cobalt (Co) and manganese (Mn) from marine nodules [29]. This involved utilizing an acid-reducing medium along with the addition of steel scrap. Table 8 contrasts the findings from Pérez et al. [29] with the outcomes of the present investigation. Notably, under similar dissolution times and conditions, except for a slightly reduced particle size in the manganese nodules in Pérez et al. [29] research, a noteworthy disparity emerges. Greater manganese extractions from the marine nodules are evident, likely attributed to their higher concentration of Fe_3O_4 in the chemical composition, thereby enhancing acid-reducing dissolution. Additionally, in line with the hypothesis put forth by [author's name], it is conceivable that the presence of gangue surrounding larger particles (Fe-Mn crusts) impedes diffusion rates. This hindrance can result in a decrease in reactant concentration, diminishing the driving force for mass transfer and consequently slowing down the reaction rate [37–39].

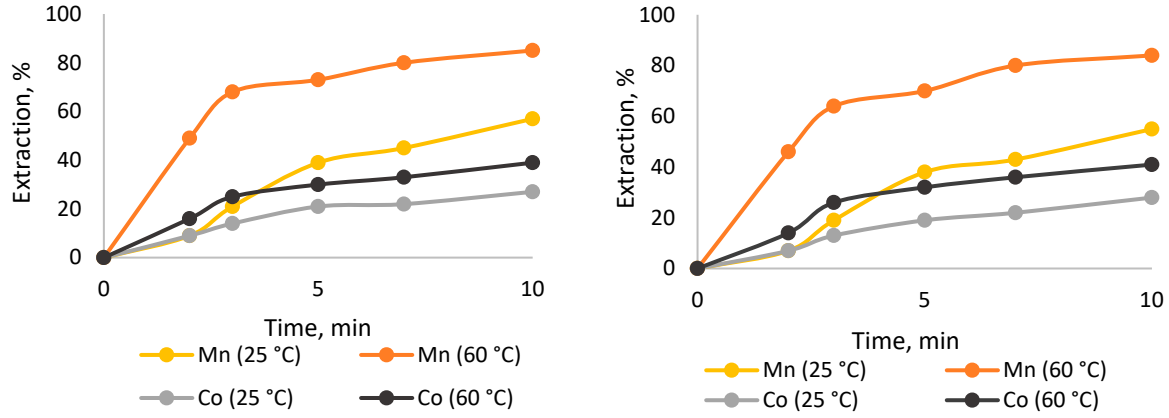

Figure 4. Manganese and cobalt extraction from ferromanganese crusts. (**A**): Drago 0511/DR04-15 (**B**): Subvent 1/DA06-4.

Table 7. Chemical concentration of Mn and Co in the solution after leaching presented in Figure 4.

	Manganese		**Cobalt**	
(A) Time (min)	25 °C Concentration (g/L)	60 °C Concentration (g/L)	25 °C Concentration (g/L)	60 °C Concentration (g/L)
2	0.01305	0,07105	0,00038	0,00068
3	0.03045	0,09860	0,00059	0,00106
5	0.05655	0.10585	0.00089	0.00127
7	0.06525	0.11600	0.00093	0.00140
10	0.08265	0.12325	0.00115	0.00166
(B) Time (min)	25 °C Concentration (g/L)	60 °C Concentration (g/L)	25 °C Concentration (g/L)	60 °C Concentration (g/L)
2	0.01099	0.07222	0.00016	0.00033
3	0.02983	0.10048	0.00031	0.00063
5	0.05966	0.10990	0.00046	0.00077
7	0.06751	0.12560	0.00053	0.00087
10	0.08635	0.13188	0.00067	0.00099

Table 8. Comparison of the dissolution of Mn and Co from marine nodules and ferromanganese crusts in an acid-reducing medium.

Experimental Conditions and Results	**Pérez et al. [29] Manganese Nodule**		**This Work Ferromanganese Crust**	
	Sample 1	**Sample 2**	**Drago 0511/DR04-15**	**Subvent 1/DA06-4**
Temperature (°C)	60	60	60	60
Particle size (µm)	−140 + 100 µm	−140 + 100 µm	−177 + 149 µm	−177 + 149 µm
Sulfuric acid concentration (mol/L)	0.1	0.1	0.1	0.1
Mineral resource/iron scrap ratio	1/2	1/2	1/2	1/2
Manganese extraction in 10 min (%)	90	87	84	85
Cobalt extraction in 10 min (%)	42	40	41	39

Regarding the redox potential and pH values, as described in previous studies [29,39], to effectively dissolve manganese in an acid-reducing medium (using iron), it is necessary to work in pH ranges from −2 to 8 and potential ranges between 1.4 and −1.2 V, while for cobalt. it is necessary to work in pH ranges from −2 to 4.5 and potential ranges between 0.8 and −0.25 V. In the results presented in Figure 5, it can be seen that for the dissolution of manganese in the two samples and temperatures studied was within a range of potential

and pH that favor the dissolution of this element, while for cobalt, it can be observed that working at room temperature (25 °C) tends to increase the potential of the system after 5 min, working in ranges that are not appropriate to effectively dissolve the Co.

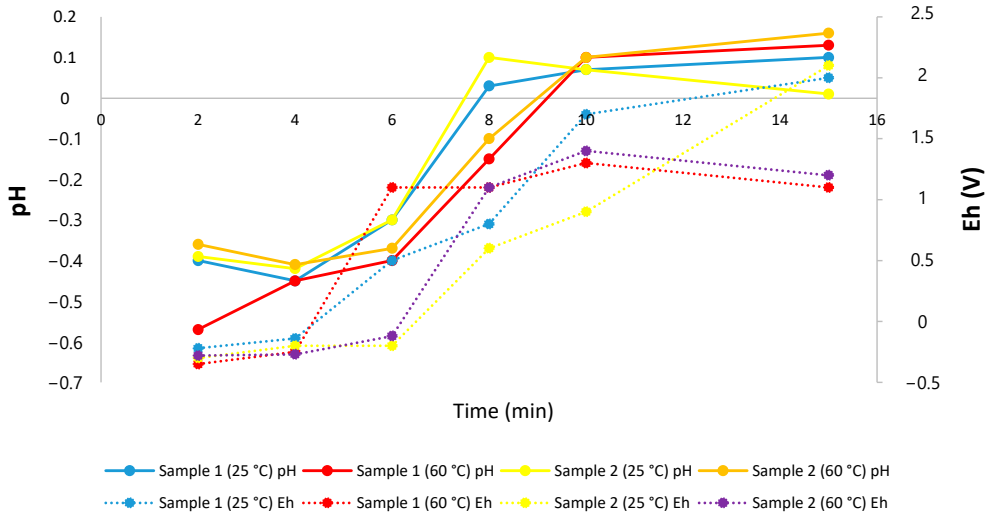

Figure 5. Effect of potential and pH on the extraction of Mn and Co from ferromanganese crusts.

3.3. Residue Analysis

The waste from the two examined samples shows an absence of contaminating elements. Moreover, as highlighted in a prior study by Toro et al. [39], the elevated concentration of ferric and ferrous ions within the system enables operation within potential redox and pH ranges conducive to manganese dissolution, thereby preventing precipitation. Additionally, a recent investigation by Pérez et al. [29] demonstrated a similar effect in the context of cobalt, affirming that working in an acid-reducing medium with high concentrations of iron yields analogous favorable outcomes.

3.3.1. Drago 0511/DR04-15

Figure 6 shows the majority composition found by SEM-EDS of Si/S/O, Fe/S/O and Fe/O, associations of impurities of Al/Si/S/O, Mg/Si/O, and Fe/O, and Mn associations found from Fe/Mg/S/O with a size range from 8.3 µm to 13.7 µm long.

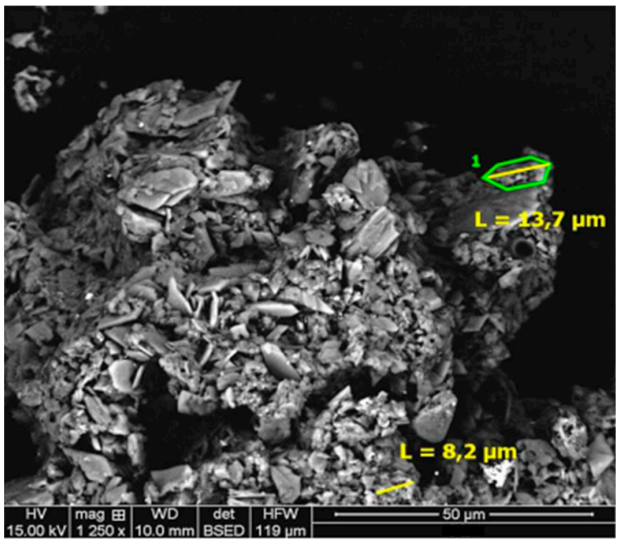

Figure 6. Scanning electron microscopy (SEM-EDS) micrograph of residue of Drago 0511/DR04-15. Magnification 1250×.

Figure 7 depicts an agglomeration of Fe/S/O particles, distinguished by red coloring in (1), green in (2), blue in (3), and green in (4). Furthermore, impurities manifest in associations such as Fe/Mn/S/O (indicated by purple coloration in (1), cyan in (2) and (3), and green in (4)), Mg/Si/O (with green coloration in (1), red in (2) and (3), and fuchsia in (4)), Si/S/O (displaying green in (1), orange in (2), fuchsia in (3), and orange in (4)), and Fe/O (red in (1), no coloration in (2), (3), or (4)) can be seen. The Fe/Mn/S/O particles exhibit lengths of 13.7 µm and 8.2 µm. Importantly, the analysis confirms the absence of contaminating elements and the non-precipitation of cobalt and manganese compounds (refer to Figure 8).

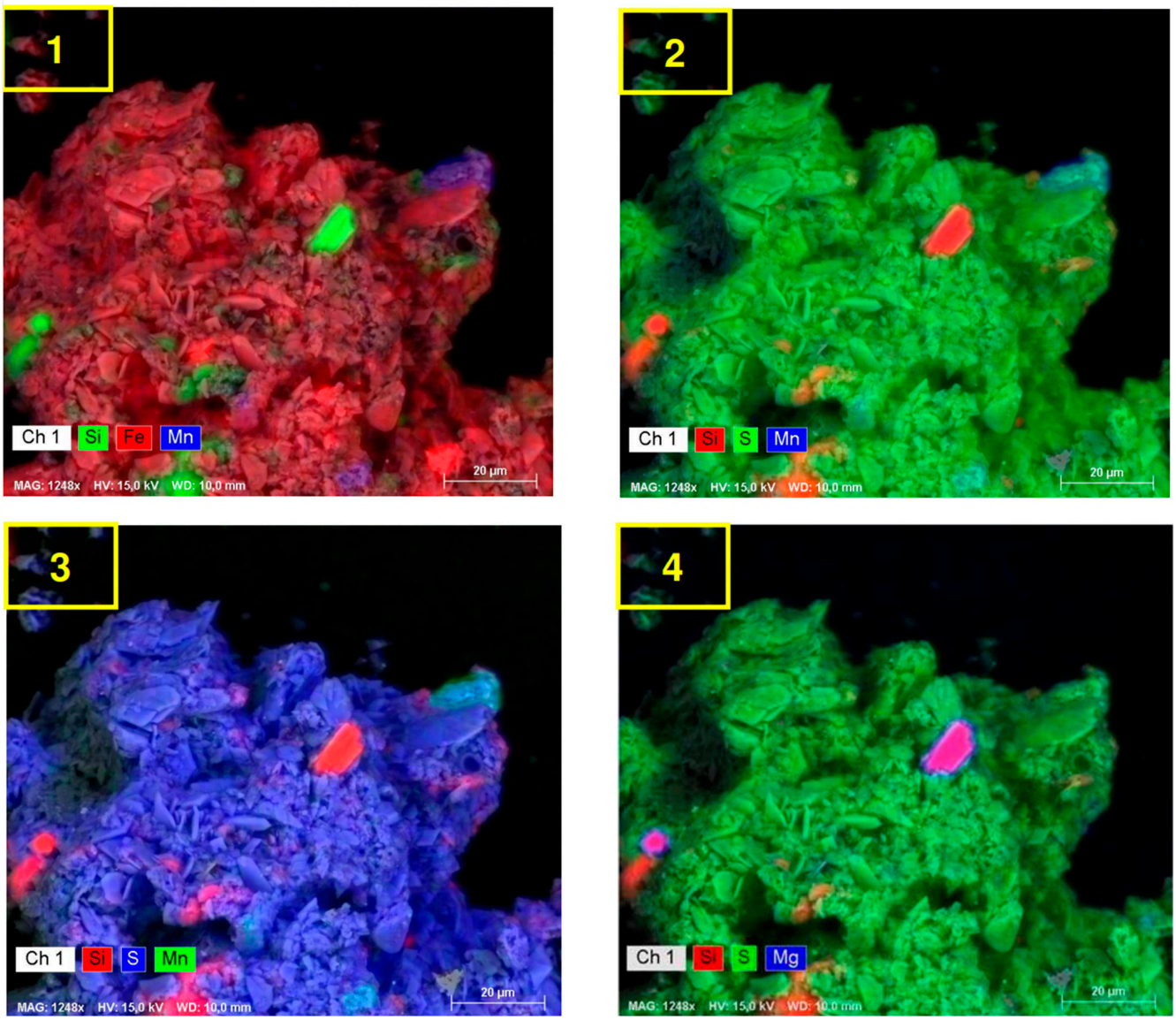

Figure 7. SEM micrograph with EDS analysis (color change) of residue Drago 0511/DR04-15. Magnification 1250× (70 µm).

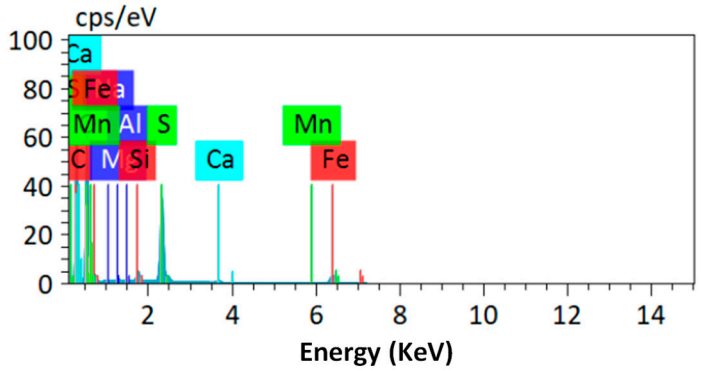

Element	Mass [%]	Mass Norm. [%]	abs. error [%] (1 sigma)
C	60,93	44,17	6,33
O	57,94	42,00	6,01
S	9,84	7,13	0,37
Fe	7,17	5,20	0,24
Si	0,92	0,67	0,06
Ca	0,48	0,35	0,04
Mn	0,29	0,21	0,03
Al	0,16	0,11	0,03
Na	0,13	0,09	0,03
Mg	0,08	0,06	0,03
	137,95	**100,00**	

Figure 8. Scanning electron microscopy elemental analysis for sample Drago 0511/DR04-15 (SEM-EDS).

3.3.2. Subvent 1/DA06-4

Figure 9 illustrates the predominant composition identified through SEM-EDS, featuring the elemental combinations of Fe/S/O and Si/S/O. Additionally, impurity associations include Si/O, Ca/S/O, Ca/Mg/Fe/Si/O, Fe/O, Al/Si/S/O, and Al/Si/O. The Mn associations are identified as Mn/S/O, ranging in size from 4.5 µm to 12.3 µm in length.

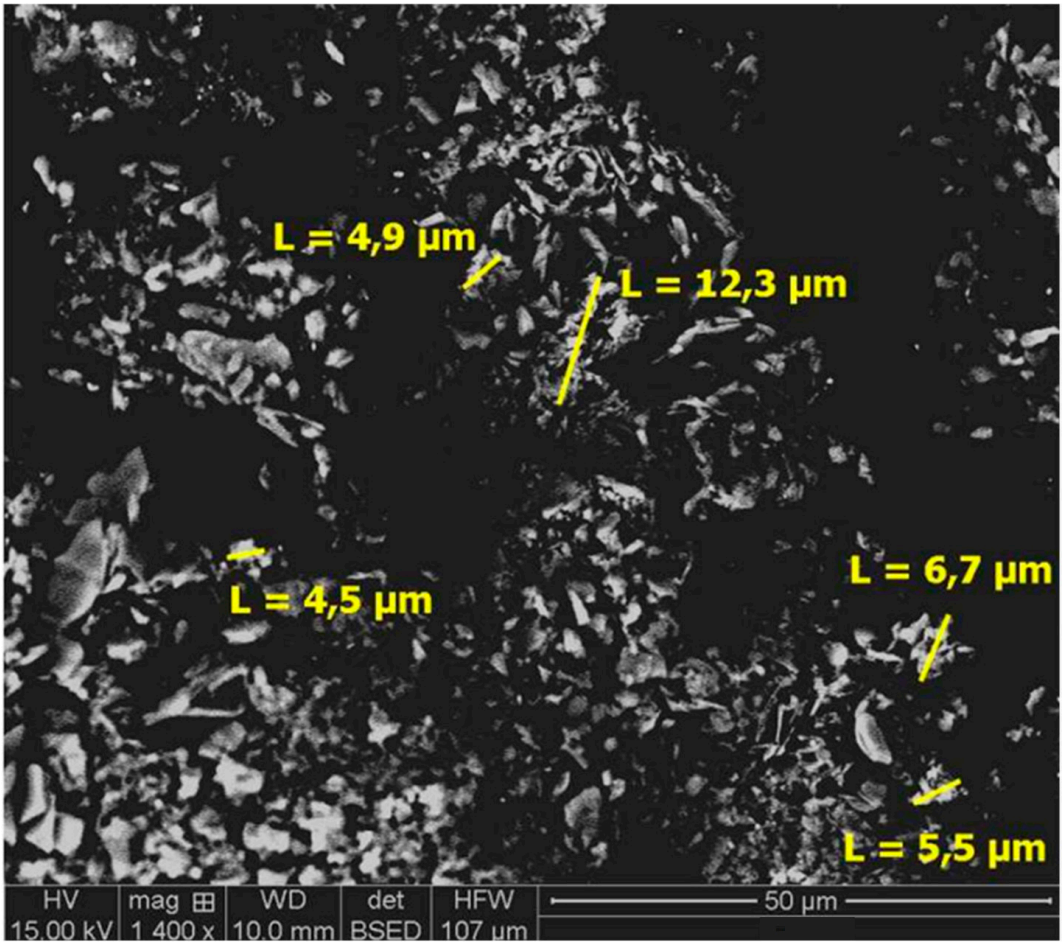

Figure 9. Scanning electron microscopy (SEM-EDS) micrograph of residue of Subvent 1/DA06-4. Magnification 1400×.

Figure 10 provides a detailed view of an agglomeration of particles featuring Fe/S/O associations, distinguished by blue coloration in (1), purple in (2), red in (3), and without coloration in (4). Within this agglomerate, impurities manifest through associations such as Mn/S/O (indicated by cyan in (1), red in (2), pink in (3), and green in (4)), Ca/S/O (with pink in (1), olive green in (2), and without coloration in (3)), Al/Si/S/O (blue in (1), red in (2), olive green in (3), and pink in (4)), Si/S/O (exhibiting blue in (1), red in (2), olive green in (3), and red in (4)), and Al/Si/O (noted by no coloration in (1) or (2), green coloration in (3), and fuchsia in (4)). The Mn/S/O particles range in size from 4.5 µm to 12.3 µm in length. Similar to sample 1, there is no evidence of contaminating element formation in this sample (refer to Figure 11).

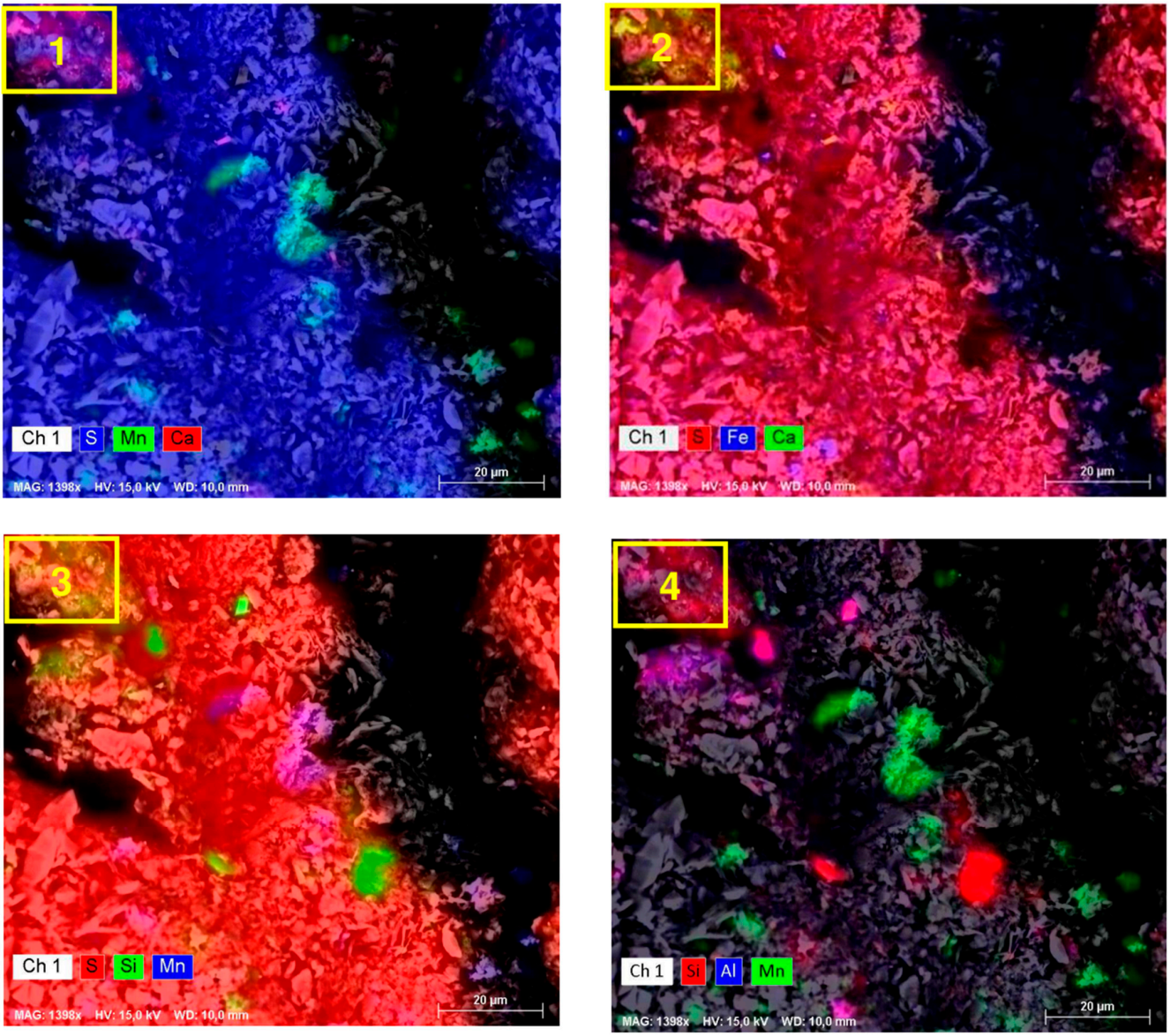

Figure 10. SEM micrograph with EDS analysis (color change) of residue Subvent 1/DA06-4. Magnification 1400× (20 µm).

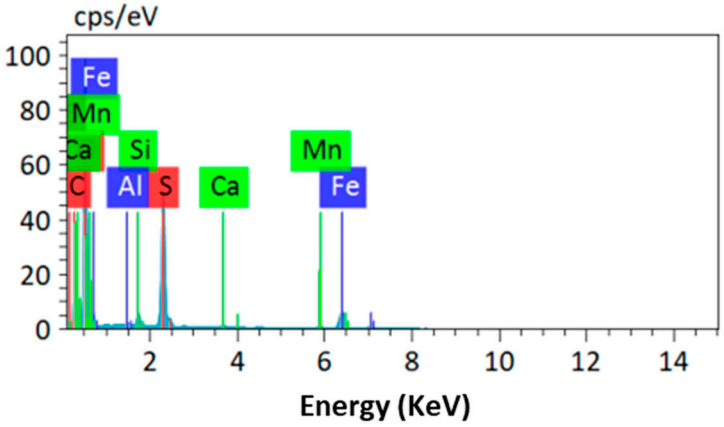

Element	Mass [%]	Mass Norm. [%]	abs. error [%] (1 sigma)
O	51,29	51,74	5,31
C	20,17	20,35	2,19
Fe	12,80	12,91	0,40
S	12,10	12,21	0,45
Mn	1,41	1,43	0,07
Si	0,87	0,87	0,06
Ca	0,38	0,38	0,04
Al	0,11	0,11	0,03
	99,13	**100,00**	

Figure 11. Scanning electron microscopy elemental analysis for sample Subvent 1/DA06-4 (SEM-EDS).

4. Conclusions

In the present investigation, the dissolution of Co and Mn was studied from two ferromanganese crusts recovered by dredge from two seamounts in the central eastern Atlantic Ocean. For this, this work was carried in an acid medium (0.1 mol/L of H_2SO_4)—reducer (steel residue (Fe-Mn crust/$Fe_{(res)}$ ratio of 1/2). at a medium temperature (25–60 °C) The main findings are detailed below.

- Studied samples have a general hydrogenic origin formed essentially by Fe-vernadite with some diagenetic influence highlighted by the presence of 10 A Mn oxides (asbolane/buserite). Fe oxyhydroxides are represented essentially by goethite-group minerals. Geochemistry reflects the mineralogy with high contents of Fe and Mn (between 15 and 20 wt. %) and great contents of several CRM as Co, Ni, Cu and REE + Y (average 3300, 2600, 900 and 2300 µg/g, respectively).
- A slight increase in the potential of the system was observed after 5 min of work at room temperature, which implies a decrease in the cobalt dissolution, because it is not possible to stably maintain the ideal redox potential range (0.8 to −0.25 V).
- The best results of this research were obtained when working at 60 °C, achieving joint extractions of Co and Mn of ~80% and ~40%, respectively, in 10 min.
- Precipitation of cobalt and manganese species is not observed in the residues studied.

In future work, it is necessary to investigate the purification of the PLS obtained in the present investigation, and in addition, the precipitation of Mn and Co. For following investigations, we put forth the technological flowchart presented in Figure 12 as an economical proposal to recover cobalt and manganese from ferromanganese crusts. In stage 1, the leaching mechanism presented in this manuscript is proposed, where Fe-Mn crust, H_2SO_4, and smelter slag are added in a stirred reactor. The product is a PLS rich in Mn and Co, which in stage 2 is put in contact with zero-valent iron (this is a good low-cost alternative, since it can be reused from metal finishing industry waste) to precipitate the manganese present in the solution. Then, in stage 3, the Co-rich PLS is concentrated (cleaned) in a solvent extraction stage, and finally in stage 4, the Co is recovered by electrowinning.

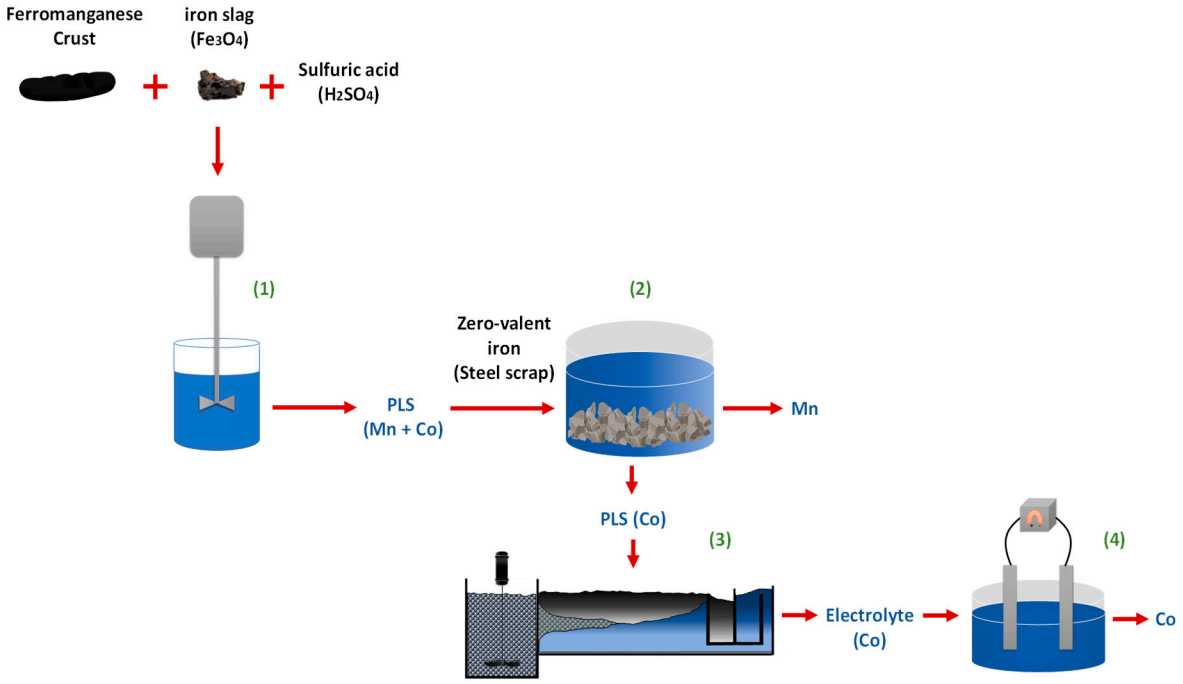

Figure 12. Technological flowchart proposal.

Author Contributions: Conceptualization, K.P. and F.M.G.M.; validation, I.J.; investigation, K.P., N.T., P.R., F.M.G.M., E.G., E.M., J.C. and P.C.H.; resources, P.R. and E.G.; writing—original draft preparation, K.P., N.T. and P.C.H.; writing—review and editing, E.G., F.J.G., E.M., J.C. and I.J.; supervision, N.T. and P.C.H.; funding acquisition, F.J.G. and E.M. All authors have read and agreed to the published version of the manuscript.

Funding: This research was funded by a European Horizon project (GSEU CL5-2021-D3-02-14, project 101075609).

Data Availability Statement: The raw data supporting the conclusions of this article will be made available by the authors on request.

Acknowledgments: Pedro Robles thanks the Fondecyt 1221702 project for supporting this investigation and the Pontificia Universidad Católica de Valparaiso for the support provided. Kevin Perez acknowledges the infrastructure and support of the PhD Program in Mineral Processes Engineering of the Universidad de Antofagasta. Felipe M. Galleguillos Madrid thanks the ANID/ FONDAP 1522A0006 Solar Energy Research Center SERC-Chile and ANID through research grant FONDECYT N° 11230550.

Conflicts of Interest: The authors declare no conflicts of interest.

References

1. Hein, J.; Conrad, T.; Staudigel, H. Seamount Mineral Deposits: A Source of Rare Metals for High-Technology Industries. *Oceanography* **2010**, *23*, 184–189. [CrossRef]
2. Cavalcanti, J.A.D.; Santos, R.V. Ferromanganese Crust: Is a Type of Cenozoic Black Stromatolite in Seabed? The Case of the Rio Grande Rise, South Atlantic Ocean. *Int. J. Paleobiol. Paleontol.* **2022**, *5*, 000129. [CrossRef]
3. Hein, J.R.; Conrad, T.A.; Dunham, R.E. Seamount Characteristics and Mine-Site Model Applied to Exploration- and Min-ing-Lease-Block Selection for Cobalt-Rich Ferromanganese Crusts. *Mar. Georesources Geotechnol.* **2009**, *27*, 160–176. [CrossRef]
4. Konstantinova, N.; Son, V.T.; Thang, L.A.; Trung, T.T.; Giang, V.T.; Dung, N.T.T.; Vanshtein, B.; Cherkashov, G. Ferro-manganese Crusts of the Vietnam Margin, Central South China Sea: Composition and Genesis. *Mar. Geol.* **2022**, *453*, 106911. [CrossRef]
5. Cronan, D.S. *Handbook of Marine Mineral Deposits*; CRC Marine Science Series, 17; CRC Press: Boca Raton, FL, USA, 2000; ISBN 084938429X.
6. Toro, N.; Gálvez, E.; Saldaña, M.; Jeldres, R.I. Submarine Mineral Resources: A Potential Solution to Political Conflicts and Global Warming. *Min. Eng.* **2022**, *179*, 107441. [CrossRef]

7. Conrad, T.; Hein, J.R.; Paytan, A.; Clague, D.A. Formation of Fe-Mn Crusts within a Continental Margin Environment. *Ore Geol. Rev.* **2017**, *87*, 25–40. [CrossRef]
8. Astakhova, N.V. Ferromanganese crusts of peter the great seamount and the vasylkovsky ridge (sea of japan). Bulletin of Kamchatka Regional Association «Educational-Scientific Center». *Earth Sci.* **2023**, *57*, 33–44. [CrossRef]
9. Sutherland, K.M.; Wankel, S.D.; Hein, J.R.; Hansel, C.M. Spectroscopic Insights Into Ferromanganese Crust Formation and Diagenesis. *Geochem. Geophys. Geosystems* **2020**, *21*, e2020GC009074. [CrossRef]
10. Baturin, G.N.; Dobretsova, I.G.; Dubinchuk, V.T. Hydrothermal Manganese Mineralization in the Peterbourgskoye Ore Field (North Atlantic). *Oceanology* **2014**, *54*, 222–230. [CrossRef]
11. Yeo, I.A.; Howarth, S.A.; Spearman, J.; Cooper, A.; Crossouard, N.; Taylor, J.; Turnbull, M.; Murton, B.J. Distribution of and Hydrographic Controls on Ferromanganese Crusts: Tropic Seamount, Atlantic. *Ore Geol. Rev.* **2019**, *114*, 103131. [CrossRef]
12. Long, B.H.; Thu, P.M.; Trung, N.N. Initial Understanding and Assessment of Role of Oceanographic Features for Ferro-manganese Crusts and Nodules in the East Vietnam Sea. *Tạp Chí Khoa Học Và Công Nghệ Biển* **2020**, *20*, 383–397. [CrossRef]
13. Ingram, B.L.; Hein, J.R.; Farmer, G.L. Age Determinations and Growth Rates of Pacific Ferromanganese Deposits Using Strontium Isotopes. *Geochim. Cosmochim. Acta* **1990**, *54*, 1709–1721. [CrossRef]
14. Toro, N.; Robles, P.; Jeldres, R.I. Seabed Mineral Resources, an Alternative for the Future of Renewable Energy: A Critical Review. *Ore Geol. Rev.* **2020**, *126*, 103699. [CrossRef]
15. Li, D.; Jiang, X.; Wang, S.; Sun, X.; Zhao, F.; Feng, L.; Zhang, D. Research on Recovery of Valuable Metals from Cobalt-Rich Crust Using Carbon as a Reduction Agent during the Acid Baking Process. *Minerals* **2022**, *12*, 1215. [CrossRef]
16. de Matos, C.S.; Benites, M.; Jovane, L.; Ulsen, C. Chemical-Mineralogical Characterization of Critical Elements into Ferromanganese Crusts. *J. Mater. Res. Technol.* **2023**, *25*, 5633–5649. [CrossRef]
17. Bruland, K.W.; Rue, E.L.; Smith, G.J. Iron and Macronutrients in California Coastal Upwelling Regimes: Implications for Diatom Blooms. *Limnol. Oceanogr.* **2001**, *46*, 1661–1674. [CrossRef]
18. Ito, M.; Hiroyoshi, N. Recent Developments in Mineral Processing of Cobalt-Rich Ferromanganese Crust/Nodules. *J. MMIJ* **2015**, *131*, 639–642. [CrossRef]
19. Konstantinova, N.; Cherkashov, G.; Hein, J.R.; Mirão, J.; Dias, L.; Madureira, P.; Kuznetsov, V.; Maksimov, F. Composition and Characteristics of the Ferromanganese Crusts from the Western Arctic Ocean. *Ore Geol. Rev.* **2017**, *87*, 88–99. [CrossRef]
20. Koschinsky, A.; Halbach, P. Sequential Leaching of Marine Ferromanganese Precipitates: Genetic Implications. *Geochim. Cosmochim. Acta* **1995**, *59*, 5113–5132. [CrossRef]
21. Benites, M.; Hein, J.R.; Mizell, K.; Jovane, L. Miocene Phosphatization of Rocks From the Summit of Rio Grande Rise, Southwest Atlantic Ocean. *Paleoceanogr. Paleoclimatol.* **2021**, *36*, e2020PA004197. [CrossRef]
22. Marino, E.; González, F.J.; Somoza, L.; Lunar, R.; Ortega, L.; Vázquez, J.T.; Reyes, J.; Bellido, E. Strategic and Rare Elements in Cretaceous-Cenozoic Cobalt-Rich Ferromanganese Crusts from Seamounts in the Canary Island Seamount Province (Northeastern Tropical Atlantic). *Ore Geol. Rev.* **2017**, *87*, 41–61. [CrossRef]
23. Toro Villarroel, N.R.; Torres Albornoz, D.A. *La Fuerza Del Litio*; Universidad Arturo Prat: Victoria, Chile, 2023; ISBN 9789564164717.
24. Lucibella, M. *APS Releases Report on Energy-Critical Elements: Critical Elements Report*; American Physical Society: Washington, DC, USA, 2011.
25. Boldy, R.; Santini, T.; Annandale, M.; Erskine, P.D.; Sonter, L.J. Understanding the Impacts of Mining on Ecosystem Services through a Systematic Review. *Extr. Ind. Soc.* **2021**, *8*, 457–466. [CrossRef]
26. Moore, K.R.; Segura-Salazar, J.; Bridges, L.; Diallo, P.; Doyle, K.; Johnson, C.; Foster, P.; Pollard, N.; Whyte, N.; Wright, O. The Out-of-This-World Hype Cycle: Progression towards Sustainable Terrestrial Resource Production. *Resour. Conserv. Recycl.* **2022**, *186*, 106519. [CrossRef]
27. Bustillo Revuelta, M. *Mineral Resources; Springer Textbooks in Earth Sciences, Geography and Environment*; Springer International Publishing: Cham, Switzerland, 2018; ISBN 978-3-319-58758-5.
28. Sharma, R. *Deep-Sea Mining: Resource Potential, Technical and Environmental Considerations*; Springer: Cham, Switzerland, 2017; pp. 1–535. [CrossRef]
29. Pérez, K.; Toro, N.; Robles, P.; Gallegos, S.; Gálvez, E.; González, F.J.; Marino, E.; Hernández, P.C. Cobalt and Manganese Extraction from Ocean Nodules by Co-Processing with Steel Metallurgical Slag. *Metals* **2023**, *13*, 1079. [CrossRef]
30. Ju, J.; Feng, Y.; Li, H.; Wu, H.; Liu, S.; Xu, C.; Li, X. Separation of Cu, Co, Ni and Mn from Acid Leaching Solution of Ocean Cobalt-Rich Crust Using Precipitation with Na2S and Solvent Extraction with N235. *Korean J. Chem. Eng.* **2022**, *39*, 706–716. [CrossRef]
31. Inoue, A.; Kawahara, M. Ammoniacal Leaching and Solvent Extraction of Cobalt Crusts Using Sulfur Dioxide Gas. *Shigen–Sozai* **1998**, *114*, 195–199. [CrossRef]
32. Nakazawa, H.; Sato, H. Bacterial Leaching of Cobalt-Rich Ferromanganese Crusts. *Int. J. Min. Process* **1995**, *43*, 255–265. [CrossRef]
33. Shibata, J.; Watari, T.; Niinae, M. Hydrochloric Acid Leaching of Cobalt-Rich Ferromanganese Crust Using Hydrogen Peroxide and Sodium Sulfite as Reducing Agents. *Shigen–Sozai* **1999**, *115*, 29–34. [CrossRef]
34. Niinae, M.; Komatsu, N.; Nakahiro, Y.; Wakamatsu, T.; Shibata, J. Preferential Leaching of Cobalt, Nickel and Copper from Cobalt-Rich Ferromanganese Crusts with Ammoniacal Solutions Using Ammonium Thiosulfate and Ammonium Sulfite as Reducing Agents. *Hydrometallurgy* **1996**, *40*, 111–121. [CrossRef]

35. Torres Albornoz, D.A. *Copper and Manganese Extraction through Leaching Processes*; Universidad Politécnica de Cartagena: Cartagena, Spain, 2021.
36. Moraga, C.; Cerecedo-Saenz, E.; González, J.; Robles, P.; Carrillo-Pedroza, F.R.; Toro, N. Comparative Study of MnO2 Dissolution from Black Copper Minerals and Manganese Nodules in an Acid Medium. *Metals* **2021**, *11*, 817. [CrossRef]
37. Zakeri, A. Dissolution Kinetics of Manganese Dioxide Ore in Sulfuric Acid in the Presence of Ferrous Ion. *Iran. J. Mater. Sci. Eng.* **2007**, *4*, 22–27.
38. Bafghi, M.S.; Zakeri, A.; Ghasemi, Z.; Adeli, M. Reductive Dissolution of Manganese Ore in Sulfuric Acid in the Presence of Iron Metal. *Hydrometallurgy* **2008**, *90*, 207–212. [CrossRef]
39. Toro, N.; Rodríguez, F.; Rojas, A.; Robles, P.; Ghorbani, Y. Leaching Manganese Nodules with Iron-Reducing Agents—A Critical Review. *Min. Eng.* **2021**, *163*, 106748. [CrossRef]